Journal of Materials Science: Materials in Electronics (2018) 29:3935–3942
https://doi.org/10.1007/s10854-017-8333-0

Promoted supercapacitive performances of electrochemically synthesized poly(3,4-ethylenedioxythiophene) incorporated with manganese dioxide

Haihan Zhou[1] · Xiaomin Zhi[1] · Hua-Jin Zhai[1]

Received: 1 September 2017 / Accepted: 25 November 2017 / Published online: 1 December 2017

Abstract
A facile electrochemical codeposition method was developed to prepare the manganese dioxide/poly(3,4-ethylenedioxythiophene) (PEDOT) composite electrodes for supercapacitor applications. Electrode characterizations include Fourier transform infrared spectroscopy, X-ray diffraction, and energy dispersive X-ray spectroscopy, indicating that the MnO_2/PEDOT composite is prepared successfully. Electrochemical tests manifest that MnO_2/PEDOT composite electrodes have better electrochemical properties than individual MnO_2 and PEDOT electrodes. The as-prepared MnO_2/PEDOT composite achieves a high areal specific capacitance of 89.7 mF cm^{-2} at 10 mV s^{-1}, as well as superior rate capability and cycle stability (maintaining 97.1% of initial capacitance for 5000 cycles). The composite we have developed also exhibits superior supercapacitive performances relative to other conducting polymers reported previously, including PEDOT based composite electrodes. These properties of MnO_2/PEDOT composite are closely related to the porous microstructures formed and the synergic effect between the two components. The present MnO_2/PEDOT based organic–inorganic hybrid materials are very promising for supercapacitor applications.

1 Introduction

With traditional fossil energy resources being exhausted gradually, the development of sustainable and highly-effective devices for energy conversion and storage has become increasingly important. Supercapacitors, also known as electrochemical capacitors, are one of the most attractive electrochemical energy storage devices due to their relatively high power and energy densities, long cycle life, and environmental friendliness [1–3], which also fill the gap between batteries and conventional capacitors [4, 5].

According to the charge storage mechanisms, supercapacitors can be categorized into electrical double-layer capacitors (EDLCs) and pseudocapacitors. Thereinto, EDLCs store energy by ionic charge separation at the electrode/electrolyte interface. For pseudocapacitors, energy is stored by fast and reversible faradaic redox reactions, which occur at the surface or near-surface of electroactive substances [6, 7]. Currently, one major obstacle that hinders the applications of supercapacitors is their relatively low energy density [8]. In contrast to EDLCs, pseudocapacitors have higher energy density because faradaic redox reactions can provide lager charge capacity. Therefore, researchers have been widely investigating the pseudocapacitive materials, including transition metal oxides and conducting polymers (CPs) [9, 10].

Among transition metal oxides, manganese dioxide (MnO_2) is considered to be one of the most promising candidates owing to its high theoretical specific capacitance, low cost, environmental benignness and abundant source [11, 12]. However, the dense morphology and poor electrical conductivity of MnO_2 (10^{-6}–10^{-5} S cm^{-1}) usually result in a low specific capacitance [13, 14]. CPs, an alternative kind of pseudocapacitive materials, are attractive because of their high faradaic pseudocapacitance. CPs have ideal intrinsic conductivity from a few to 500 S cm^{-1} under the doped state. In particular, poly(3,4-ethylenedioxythiophene) (PEDOT) exhibits higher electrical conductivity (300–500 S cm^{-1}) as compared to other CPs, such as polypyrrole (PPy) and

✉ Haihan Zhou
hhzhou@sxu.edu.cn

✉ Hua-Jin Zhai
hj.zhai@sxu.edu.cn

[1] Institute of Molecular Science, Key Laboratory of Materials for Energy Conversion and Storage of Shanxi Province, Key Laboratory of Chemical Biology and Molecular Engineering of Education Ministry, Shanxi University, Taiyuan 030006, China

polyaniline (PANI) [15]. Consequently, the composites containing MnO_2 and PEDOT, a kind of organic–inorganic hybrid materials, are actively pursued as promising pseudocapacitor electrode materials. For instance, Tang et al. [16] and Hu et al. [17] prepared composite electrodes based on PEDOT and MnO_2 via step-by-step anodic deposition on nickel foam and carbon fiber derived from ramie, respectively. Liu et al. [18] fabricated MnO_2/PEDOT coaxial nanowires by using anodic aluminum oxide (AAO) template. Sen et al. [19] synthesized MnO_2/PEDOT by reverse microemulsion non-aqueous polymerization, which involves multistep redox reactions. Kim et al. [20] fabricated MnO_2/PEDOT nanowires by galvanic displacement reaction. Yang et al. [21] constructed MnO_2/PEDOT composite by thermal treatment and chemical vapor polymerization.

Although the above-mentioned MnO_2/PEDOT composites [16–21] show good electrochemical capacitive properties, the preparation methods have limitations such as harsh experiment conditions (corrosive reagents and high temperature), fragility and time-consuming removal of AAO template, and complicated multiple-step procedures. Therefore, there is a demand in the development of a simpler, facile, and cost-effective method for high performance MnO_2/PEDOT composite electrodes. In addition, almost all relevant researches focus on the gravimetric specific capacitance of electrode materials. When supercapacitors are used for small scale electronics and energy storage of stationary devices, areal specific capacitance is a better performance indicator [22, 23]. For this purpose, the present study of MnO_2/PEDOT electrodes will focus on specific capacitance in area units.

Here we propose a simple and facile one-pot electrochemical method to deposit MnO_2/PEDOT composite on graphite foil substrate. For comparison, individual MnO_2 and PEDOT electrodes are also prepared using the same procedure. Electrochemical capacitive properties of the three types of electrodes are investigated using cyclic voltammetry (CV), galvanostatic charge/discharge (GCD) measurements, and electrochemical impedance spectroscopy (EIS). Supercapacitive performances of the MnO_2/PEDOT composite electrodes are also compared with those of other CP based composites in the literature in terms of areal specific capacitance.

2 Experimental

2.1 Electrode preparation

Commercial graphite foil was cut into a rectangular shape and insulated with adhesive tape to expose conductive areas of 1 cm × 1 cm as the substrate for electrodeposition. To remove surface defects and contamination, the exposed substrate was successively polished with fine sandpaper, etched in a 20 wt% H_2SO_4 solution for 1 min, and dipped into acetone for 30 s. Prior to use, the graphite foil was cleaned with deionized water and dried in a vacuum oven at 60 °C for several hours.

The MnO_2/PEDOT composite was co-electrodeposited on graphite foil with a standard three-electrode system in the deposition bath containing 0.01 M EDOT monomer, 0.01 M $MnSO_4$, and 0.1 M KCl. The deposition bath was produced by dissolving the above chemical reagents in deionized water under ultrasonication for about 15 min. All chemicals were analytical grade and used as-received. For the electrodeposition, a saturated calomel electrode (SCE) was used as the reference electrode and a platinum sheet with large area as the counter electrode. Electrodeposition was performed at a constant potential of 1.0 V versus SCE for 40 min. After deposition, the MnO_2/PEDOT composite electrode was rinsed with deionized water to remove unreacted substance. For comparison, MnO_2 electrode was prepared with the same procedure in the deposition bath containing 0.01 M $MnSO_4$ and 0.1 M KCl. PEDOT electrode was prepared in the deposition bath consisting of 0.01 M EDOT monomer and 0.1 M H_2SO_4 under the same electrodeposition condition.

2.2 Characterizations

Fourier transform infrared (FT-IR) spectroscopy and X-ray diffraction (XRD) were performed using Bruker Tensor 27 FT-IR spectrometer and Rigaku Ultima IV X-ray diffractometer, respectively. The morphology of samples was observed by a field emission scan electron microscope (FE-SEM, JSM-6701F, JEOL) and a high-resolution transmission electron microscopy (HRTEM, Tecnai G2 F20, FEI). Energy dispersive X-ray spectroscopy (EDS) was measured using a SEM (S-4800, Hitachi) equipped with an X-ray energy dispersive spectrometer. For the FT-IR, XRD, and TEM characterizations, the samples were scraped from the deposit coated conducting glasses, because it would scrape off graphite when scraping from the surface of the deposit coated graphite foils.

Electrochemical capacitive properties of as-prepared electrodes were measured using a two-electrode system, which was composed of two pieces of identical deposit coated graphite foils, with a sandwiched filter paper soaked with 1.0 M KCl aqueous solution as the separator. The CV, GCD, and EIS tests were conducted with an electrochemical workstation (CHI 660E, Chenhua, China). The EIS curves were measured at a frequency range from 10^5 to 10^{-2} Hz using a 5 mV (rms) AC sinusoid signal referring to the open circuit potential.

3 Results and discussion

3.1 Component analyses and morphology

The resulting MnO_2, PEDOT, and MnO_2/PEDOT composite materials were characterized by FT-IR, which are shown in Fig. 1a. For MnO_2, the band at 1630 cm^{-1} is related to the O–H vibration of absorbed water. Peaks at 746, 522, and 467 cm^{-1}, which are below 750 cm^{-1}, are ascribed to Mn–O vibrations of MnO_6 octahedra in α-MnO_2 [24, 25]. In the spectrum of PEDOT, vibrations at 1517 and 1355 cm^{-1} correspond to C=C and C–C stretchings, respectively, of the quinoid structure in the thiophene ring [26]. The absorption peaks at 1203, 1144, and 1090 cm^{-1} are attributed to C–O–C stretching in the ethylenedioxy group [27]. Additionally, the vibrations of C–S bond in the thiophene ring are observed at 983, 841, and 692 cm^{-1} [28]. For MnO_2/PEDOT, it can be seen that both of the above characteristic peaks originated from PEDOT (black font) and MnO_2 (red font) exist, indicating the formation of MnO_2/PEDOT composite.

The crystal phases of as-prepared electrode materials were investigated by XRD. Figure 1b shows the XRD patterns of MnO_2, PEDOT, and MnO_2/PEDOT. For MnO_2, there are three diffraction peaks at 25.7° (220 plane), 37° (211 plane), and 65.6° (002 plane), which can be indexed to α-MnO_2 (JCPDS card No. 44-0141) [29, 30]. The intensity of these peaks is weak and broad, indicating a small degree of crystallization for electrodeposited MnO_2. For PEDOT, the diffraction peak located at 26° originates from the (020) plane of PEDOT [31]. In the case of MnO_2/PEDOT, the diffraction peak of PEDOT and those of (211) and (002) planes of α-MnO_2 are observed. The XRD tests further indicate that MnO_2/PEDOT composite was successfully prepared through a facile one-pot electrochemical method. Moreover, from the EDS pattern (Fig. 1c), atomic ratio of C:O:S:Mn in the composite is 47.9:38.1:1.8:12.2.

Surface morphology of electrode materials is a critical factor that affects their supercapacitive properties. The top panels of Fig. 2 show the SEM images of MnO_2, PEDOT, and MnO_2/PEDOT. We can see that MnO_2 presents a dense fibrillar morphology, where nanofibers accumulate together. Also a morphology of compact polymer is observed for PEDOT. However, the MnO_2/PEDOT composite has loose and porous microstructures, which are markedly different from those of PEDOT. This difference appears to be due to the incorporation of MnO_2. As indicated by the arrows, MnO_2 is anchored within the PEDOT matrix. Such favourable porous microstructures shorten the diffusion path of electrolyte, enabling electrolyte to penetrate easily to the inner of the composite. Consequently, MnO_2 and PEDOT

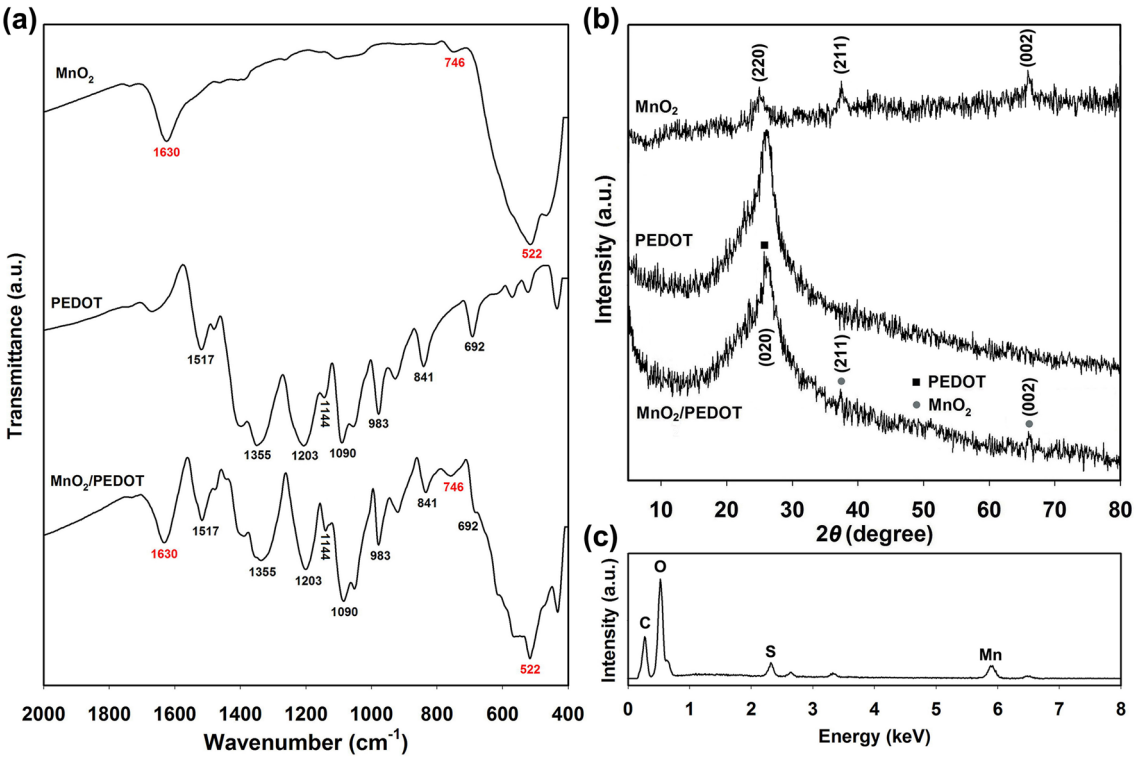

Fig. 1 **a** FT-IR spectra and **b** XRD patterns of MnO_2, PEDOT, and MnO_2/PEDOT composite electrodes; **c** EDS of MnO_2/PEDOT composite

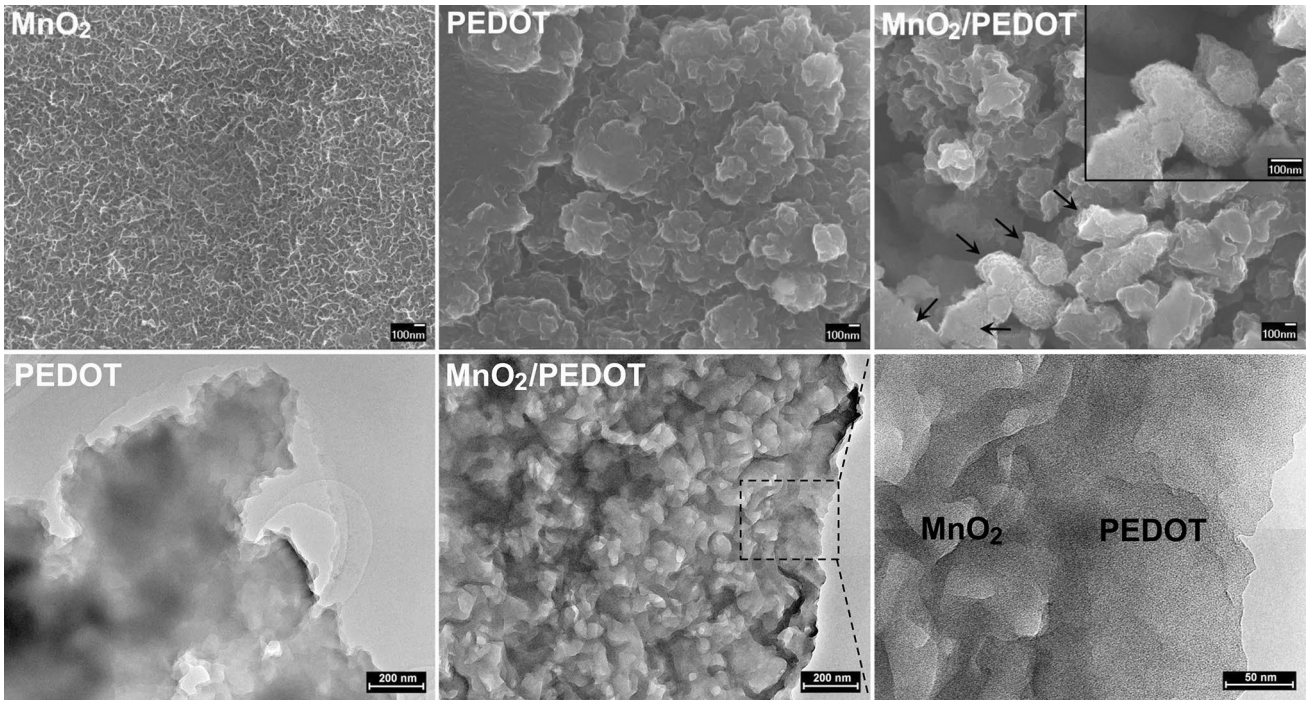

Fig. 2 SEM images (top panels) of MnO_2, PEDOT, and MnO_2/PEDOT composite electrodes. In MnO_2/PEDOTMnO_2 composite, MnO_2 anchored within PEDOT matrix is marked with black arrows and the inset in the image shows MnO_2 at higher magnification. Bottom panels are TEM images of PEDOT and MnO_2/PEDOT electrodes

in MnO_2/PEDOT composite can both be adequately utilized for electrochemical energy storage.

The bottom panels of Fig. 2 show TEM images of PEDOT and MnO_2/PEDOT. Using the image of PEDOT as a reference, it is seen in MnO_2/PEDOT composite that MnO_2 is anchored on PEDOT, even though the composite has suffered from long time ultrasonication during sample preparation for TEM tests. This observation indicates that MnO_2 and PEDOT within MnO_2/PEDOT composite have rather strong interactions. In short, the MnO_2/PEDOT composite exhibits porous microstructures with strong interactions between individual components, which should lead to good synergic effect between MnO_2 and PEDOT. To be specific, highly conductive PEDOT helps make up the disadvantage of MnO_2 for poor electrical conductivity, whereas MnO_2 with high theoretical specific capacitance promotes the capacitance properties of PEDOT. Consequently, the MnO_2/PEDOT composite is anticipated for superior electrochemical capacitive properties with respect to its individual components; see below.

3.2 Electrochemical properties

Supercapacitive behaviors of MnO_2, PEDOT, and MnO_2/PEDOT electrodes were evaluated using a two-electrode system, which allows a better assessment of the materials for practical supercapacitor applications [32]. Figure 3a shows the CV curves at 10 mV s^{-1} of MnO_2, PEDOT, and MnO_2/PEDOT electrodes. It is obvious that the shape of CV curve of MnO_2 electrodes deviates from rectangle, indicative of its unsatisfactory supercapacitive nature. The PEDOT electrodes show the shape closer to rectangle. Remarkably, the MnO_2/PEDOT composite electrodes exhibit a nearly perfect rectangular shape. Moreover, as shown in Fig. 3b, the rectangle-like CV curves show almost symmetric *I–E* responses up to 200 mV s^{-1} and the current density persistently increases at higher scan rate, demonstrating that MnO_2/PEDOT composite has superior rate capability, a key specification for supercapacitors.

Areal specific capacitance (C_S) of electrodes can be calculated from the CV curves using the following equation:

$$C_S = \left(\int IdV \right) / (S \times \Delta V \times v) \quad (1)$$

where C_S represents the areal specific capacitance in F cm^{-2}; $\int I\,dV$ the integrated area of the CV curve; S the geometric surface area of electrode in cm^2, which is fixed to 1 cm^2 in this research; ΔV the scanning potential window in V; and v the scan rate in V s^{-1}. As shown in Fig. 3c, MnO_2/PEDOT electrodes have the largest specific capacitance at all scan rates, manifesting that they have superior electrochemical capacitive properties as compared to individual MnO_2 and PEDOT electrodes. The MnO_2/PEDOT electrodes achieve

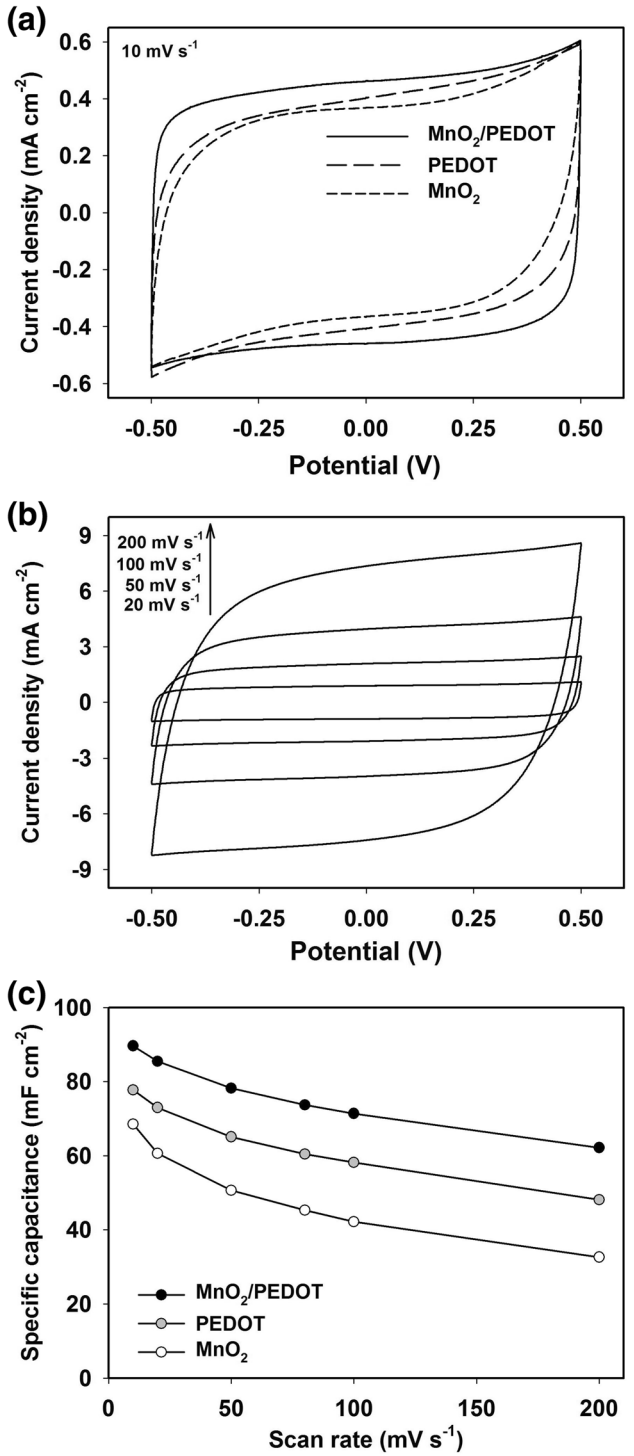

Fig. 3 **a** CV curves at the scan rate of 10 mV s^{-1} for MnO_2, PEDOT, and MnO_2/PEDOT composite electrodes. **b** CV curves at the scan rate range from 50 to 200 mV s^{-1} for MnO_2/PEDOT composite electrodes. **c** Relationship of areal specific capacitance with CV scan rate for MnO_2, PEDOT, and MnO_2/PEDOT composite electrodes

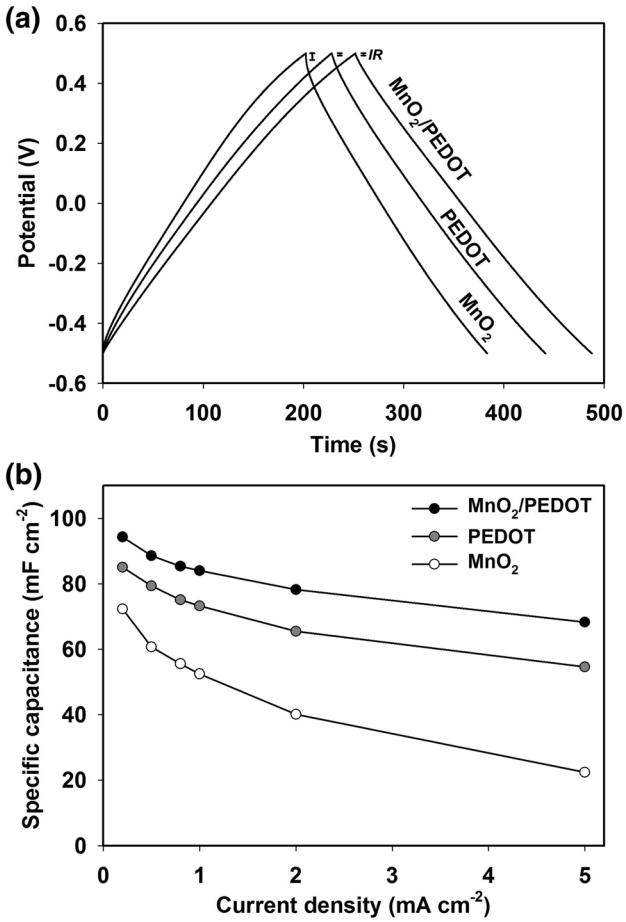

Fig. 4 **a** GCD curves at current density of 0.2 mA cm^{-2} and **b** plots of specific capacitance versus GCD current density for MnO_2, PEDOT, and MnO_2/PEDOT composite electrodes

a specific capacitance of 89.7 mF cm^{-2} at 10 mV s^{-1}, which is higher than those of CP based composites in literature: TiO_2/PPy (64.6 mF cm^{-2} at 10 mV s^{-1}) and graphene oxide/PEDOT (66.3 mF cm^{-2} at 10 mV s^{-1}) [33, 34].

GCD measurements were conducted to further compare the performances of MnO_2, PEDOT, and MnO_2/PEDOT electrodes. As shown in Fig. 4a, the three types of electrodes exhibit triangle-shaped GCD curves, with MnO_2/PEDOT composite electrodes having the longest discharge time. Also, MnO_2/PEDOT electrodes show an observably lower *IR* drop with respect to MnO_2 and PEDOT electrodes, which suggests that the tested supercapacitor cell assembled with MnO_2/PEDOT electrodes has an obviously smaller internal resistance. It is stressed that a low internal resistance is importance for energy-storing devices, because it will save energy by avoiding the production of unwanted heat during the charging/discharging processes [35].

On the basis of GCD curves, areal specific capacitance of electrodes can be obtained from the equation:

$$C_S = (2 \times I \times t)/(S \times \Delta V) \quad (2)$$

where C_S is the areal specific capacitance in F cm^{-2}, I the discharge current in A, t the discharge time in s, S the geometric surface area of electrode (fixed as 1 cm^2 in this study), and ΔV the scanning potential window in V. It can be observed from Fig. 4b that the MnO_2/PEDOT electrodes have the highest specific capacitance at all GCD current densities, in line with the CV results. Here, MnO_2/PEDOT electrodes delivery a large areal capacitance of 94.3 mF cm^{-2} at 0.2 mA cm^{-2}. This value is to be compared with those of the CP based electrode materials reported previously, such as 3D porous graphene/PANI composite (67.2 mF cm^{-2} at 0.05 mA cm^{-2}), Prussian blue/PEDOT (40.0 mF cm^{-2} at 0.45 mA cm^{-2}), and graphite oxide/PANI composite (6.3 mF cm^{-2} at 0.16 mA cm^{-2}) [36–38]. Note that the specific capacitance of MnO_2/PEDOT electrodes shows a slow and relatively smooth decline with the increase of current density, retaining 72.4% of initial capacitance when the current density is increased by as much as 25 times (68.3 mF cm^{-2} at 5 mA cm^{-2}). For comparison, when current density increases from 0.2 to 5 mA cm^{-2}, PEDOT electrodes keep 64.2% of initial capacitance, while MnO_2 electrodes only maintain 30.9%. This trend indicates that MnO_2/PEDOT composite electrodes have effectively promoted rate capability with respect to its individual components.

As a powerful tool, EIS is used to evaluate charge transport at the electrode/electrolyte interface and ion diffusion within electroactive substances. Figure 5 illustrates the Nyquist plots of MnO_2, PEDOT, and MnO_2/PEDOT electrodes. Capacitive character can be observed for these three types of electrodes, because all of them display a vertical trend for impedance plots at low frequencies. Nevertheless, in the low frequency region, the straight line of MnO_2/PEDOT electrodes leans more towards the imaginary axis with respect to MnO_2 and PEDOT electrodes, indicating better capacitive behavior for MnO_2/PEDOT [39]. Equivalent series resistance (ESR) is an important parameter that can be obtained at high frequency, which is associated with the electrolyte solution resistance, the intrinsic resistance of active materials, and the interfacial contact resistance between active materials and current collectors [40]. It can be determined by the intercept at the x-axis in EIS plot. The inset in Fig. 5 shows that, compared to MnO_2 and PEDOT electrodes, the MnO_2/PEDOT electrodes have the smallest ESR, which is beneficial to electrochemical energy-storing devices.

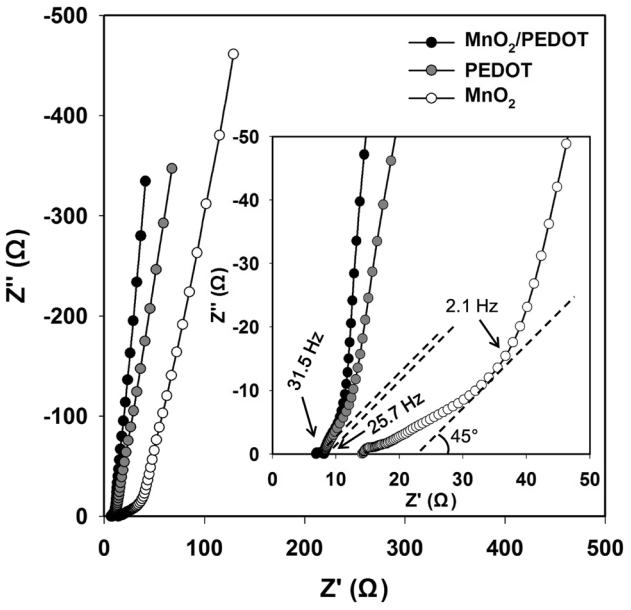

Fig. 5 Nyquist plots of MnO_2, PEDOT, and MnO_2/PEDOT composite electrodes. The insert shows the EIS curves in the high-frequency region

The knee frequency (f_{knee}) is introduced to further compare the electrode processes for the three types of electrodes. It is the maximum frequency at which predominant capacitive behavior is maintained, determined by the crossing of Warburg-type line (inclined 45°) and low-frequency vertical line. Higher knee frequency means faster charge transfer rates and lower ionic diffusion impedance [39, 41]. We can see from the inset of Fig. 5 that MnO_2/PEDOT composite electrodes exhibit higher f_{knee} (31.5 Hz) than those of PEDOT (25.7 Hz) and MnO_2 electrodes (2.1 Hz), further indicating that the composite electrodes have better charge transfer and ion diffusion of electrolyte. The EIS tests also demonstrate that MnO_2/PEDOT electrodes have superior capacitive behavior with respect to MnO_2 and PEDOT electrodes, which agrees well with CV and GCD data. As described in morphology characterizations, the enhanced supercapacitive properties for MnO_2/PEDOT composite can be attributed to the porous microstructures and the synergic effect between the individual components.

3.3 Cycle performance and Ragone plot

Cycle life is a key index for supercapacitor electrodes in practical use. In this study, the cycle stability of electrodes was assessed for 5000 CV cycles at the scan rate of 80 mV s^{-1}. As shown in the inset of Fig. 6a, the CV curve of cycle 5000 is almost identical to that of cycle 1 for the MnO_2/PEDOT electrodes, maintaining 97.1% of initial capacitance after 5000 cycles. Furthermore, it can be also seen from Fig. 6b that the MnO_2/PEDOT composite maintains the unchanged loose and porous microstructure after 5000 cycles. In contrast, PEDOT and MnO_2 electrodes retain 89.3 and 68.8%, respectively. The above numbers suggest that the cycle life of MnO_2 electrodes is markedly extended after incorporating with PEDOT in the MnO_2/PEDOT electrodes. Previous studies have suggested that active materials dissolve during electrochemical cycling, which accounts

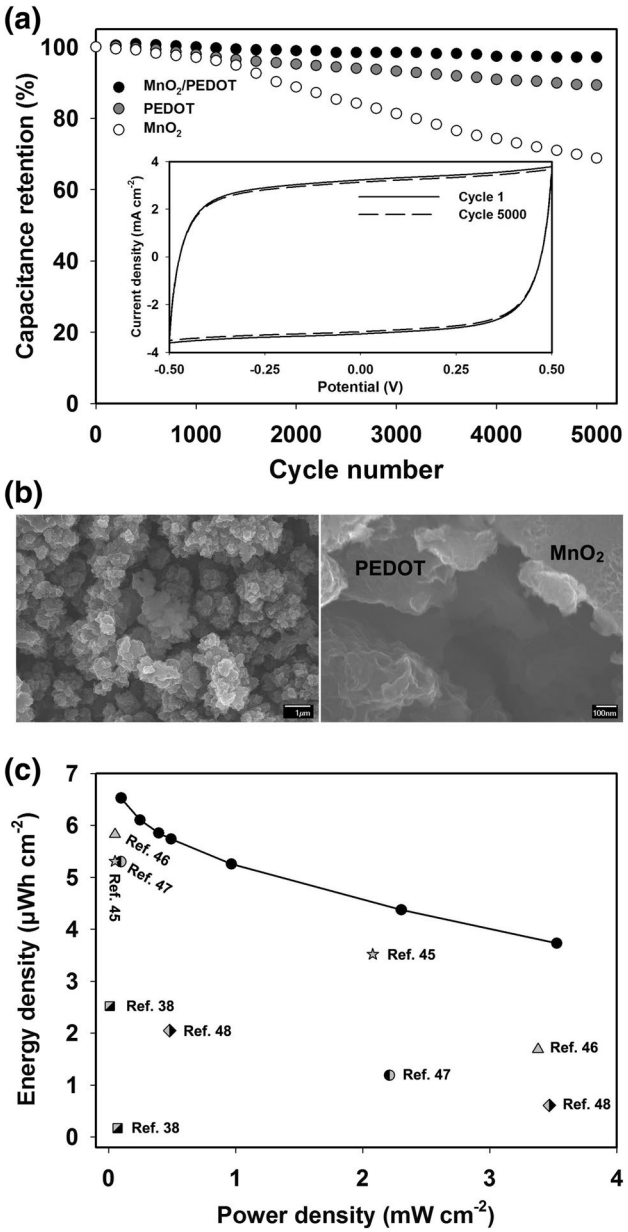

Fig. 6 **a** Relationship of capacitance retention and cycle number for MnO_2, PEDOT, and MnO_2/PEDOT composite electrodes. The inset shows CV curves of MnO_2/PEDOT at cycle 1 and cycle 5000; **b** SEM images of MnO_2/PEDOT composite electrodes after cycling test at different magnifications; **c** Ragone plot of supercapacitor composed of MnO_2/PEDOT composite electrodes, as compared with data from previous supercapacitors composed of CP based composite electrodes

for major capacitance loss of MnO_2 electrodes [42, 43]. An effective route to prevent MnO_2 from electrochemical dissolution is to introduce other active materials as an effective barrier to Mn cation permeation while allowing electrolyte to be accessible [44]. We believe PEDOT within MnO_2/PEDOT composite plays the role of an effective barrier to protect MnO_2 from dissolution. Consequently, the cycle life of MnO_2 electrodes is markedly extended. Likewise, it is possible that the incorporated MnO_2 may partially prevents PEDOT from swelling and shrinking during cycling, which explains why the composite electrodes also have better cycling stability than individual PEDOT electrodes.

Areal specific energy density and power density of the supercapacitor composed of two pieces of identical MnO_2/PEDOT electrodes can be obtained from Eqs. (3) and (4) [34, 38], respectively:

$$E = \frac{\frac{1}{2}C_S \Delta V^2}{3600} \tag{3}$$

$$P = \frac{3600E}{\mathrm{t}} \tag{4}$$

where E is the areal specific energy density in Wh cm^{-2}; P the areal specific power density in W cm^{-2}; C_S the areal specific capacitance of supercapacitor in F cm^{-2}; ΔV is the potential window subtracting IR drop in V; t the discharge time in s; and 3600 is for unit conversion between second and hour. Figure 6c shows the Ragone plot of the supercapacitor composed of MnO_2/PEDOT electrodes. It achieves the highest power density of 3.5 mW cm^{-2} and the maximum energy density of 6.5 μWh cm^{-2}, which are higher than the CP based supercapacitors: PEDOT/poly(styrene sulfonate) [45], PEDOT/sodium dodecyl sulfate [46], PEDOT/graphene oxide [47], PANI/graphite oxide [38], PPy/carbon paper [48], and so on.

In short, compared with individual MnO_2 and PEDOT electrodes, the enhanced supercapacitive performances for MnO_2/PEDOT composite electrodes can be ascribed to the porous microstructures formed, in which strong interactions are present between individual components. This shortens the diffusion path of electrolyte and enables easily penetration of electrolyte to the inner of the composite. Consequently, electroactive materials containing MnO_2 and PEDOT can be adequately utilized in MnO_2/PEDOT composite electrodes. Also, better synergic effect between MnO_2 and PEDOT due to their strong interactions is anticipated to boost the supercapacitive performances. Highly conductive PEDOT helps make up the disadvantage of MnO_2 for poor electrical conductivity, whereas MnO_2 with high theoretical specific capacitance promotes the capacitance properties of PEDOT.

4 Conclusions

We have fabricated MnO_2/PEDOT composite electrodes through a facile method of electrochemical co-deposition. The MnO_2/PEDOT electrodes show effectively improved electrochemical capacitive properties relative to the

individual components. The composite electrodes also show superior supercapacitive performances comparing to other CP based composite materials in the literature. The prepared composite electrodes not only achieve a high areal specific capacitance of 89.7 mF cm^{-2} at 10 mV s^{-1}, but also show superior rate capability and cycle stability (maintaining 97.1% of initial capacitance for 5000 cycles). These observations are associated to the porous microstructures of the composite and the synergic effect of MnO_2 and PEDOT. The MnO_2/PEDOT composite we have prepared, with ideal supercapacitive properties and cycle stability, is promising for uses in low-cost and high performance electrochemical energy-storing devices.

Acknowledgements This work was supported by the National Natural Science Foundation of China (21601113 and 21573138), the Natural Science Foundation of Shanxi Province (2015021079), the China Postdoctoral Science Foundation (2015M571283), the Scientific and Technological Innovation Programs of Higher Education Institutions in Shanxi (2017112), and the Sanjin Scholar Distinguished Professors Program.

References

1. X. Peng, H.L. Liu, Q. Yin, J.C. Wu, P.Z. Chen, G.Z. Zhang, G.M. Liu, C.Z. Wu, Y. Xie, Nat. Commun. **7**, 11782 (2016)
2. C. Xu, Z.H. Li, C. Yang, P.C. Zou, B.H. Xie, Z.Y. Lin, Z.X. Zhang, B.H. Li, F.Y. Kang, C.P. Wong, Adv. Mater. **28**, 4105–4110 (2016)
3. J. Yang, C. Yu, X.M. Fan, S.X. Liang, S.F. Li, H.W. Huang, Z. Ling, C. Hao, J.S. Qiu, Energy Environ. Sci. **9**, 1299–1307 (2016)
4. M. Caglar, A. Arslan, R. Kilic, E. Hur, Synth. Met. **206**, 8–14 (2015)
5. Y. Chen, Z.L. Zhang, Z.J. Sui, Z.T. Liu, J.H. Zhou, X.G. Zhou, Int. J. Hydrog. Energy **41**, 12136–12145 (2016)
6. Q.Y. Lv, S. Wang, H.Y. Sun, J. Luo, J. Xiao, J.W. Xiao, F. Xiao, S. Wang, Nano Lett. **16**, 40–47 (2016)
7. P.S. Yang, L. Ma, M.Y. Gan, Y. Lei, X.L. Zhang, M. Jin, G. Fu, J. Mater. Sci. Mater. Electron. **28**, 7333–7342 (2017)
8. Y.C. Zhao, C.A. Wang, Mater. Des. **97**, 512–518 (2016)
9. Z.H. Li, M.F. Shao, L. Zhou, R.K. Zhang, C. Zhang, J.B. Han, M. Wei, D.G. Evans, X. Duan, Nano Energy **20**, 294–304 (2016)
10. E.G. Tolstopjatova, S.N. Eliseeva, A.O. Nizhegorodova, V.V. Kondratiev, Electrochim. Acta **173**, 40–49 (2015)
11. Z.P. Bai, H.J. Li, M.J. Li, C.P. Li, X.F. Wang, C.Q. Qu, B.H. Yang, Int. J. Hydrog. Energy **40**, 16306–16315 (2015)
12. B. Ke, J.X. Wang, D.R. Li, S.Q. Zhao, L.J. Luo, L. Yu, S. Hussain, J. Mater. Sci. Mater. Electron. **28**, 418–425 (2017)
13. S.X. Deng, D. Sun, C.H. Wu, H. Wang, J.B. Liu, Y.X. Sun, H. Yan, Electrochim. Acta **111**, 707–712 (2013)
14. Y.J. Li, G.L. Wang, K. Ye, K. Cheng, Y. Pan, P. Yan, J.L. Yin, D.X. Cao, J. Power Sources **271**, 582–588 (2014)
15. G.A. Snook, P. Kao, A.S. Best, J. Power Sources **196**, 1–12 (2011)
16. P.Y. Tang, Y.Q. Zhao, C.L. Xu, Electrochim. Acta **89**, 300–309 (2013)
17. X. Hu, W. Xiong, W. Wang, S.L. Qin, H.Y. Cheng, Y. Zeng, B. Wang, Z.H. Zhu, ACS Sustain. Chem. Eng. **4**, 1201–1211 (2016)
18. R. Liu, S.B. Lee, J. Am. Chem. Soc. **130**, 2942–2943 (2008)
19. P.T. Sen, A. De, A.D. Chowdhury, S.K. Bandyopadhyay, N. Agnihotri, M. Mukherjee, Electrochim. Acta **108**, 265–273 (2013)
20. K.H. Kim, J.Y. Kim, K.B. Kim, J. Electroceram **29**, 149–154 (2012)
21. Y.J. Yang, W.T. Yuan, S.B. Li, X.J. Yang, J.H. Xu, Y.D. Jiang, Electrochim. Acta **165**, 323–329 (2015)
22. J.P. Liu, J. Jiang, M. Bosman, H.J. Fan, J. Mater. Chem. **22**, 2419–2426 (2012)
23. Y.Y. Horng, Y.C. Lu, Y.K. Hsu, C.C. Chen, L.C. Chen, K.H. Chen, J. Power Sources **195**, 4418–4422 (2010)
24. T. Gao, M. Glerup, F. Krumeich, R. Nesper, H. Fjellvag, P. Norby, J. Phys. Chem. C **112**, 13134–13140 (2008)
25. H.G. Wang, Z.G. Lu, D. Qian, Y.J. Li, W. Zhang, Nanotechnology **18**, 115616 (2007)
26. Y.Q. Han, B. Ding, H. Tong, X.G. Zhang, J. Appl. Polym. Sci. **121**, 892–898 (2011)
27. H.J. Shin, S.S. Jeon, S.S. Im, Synth. Met. **161**, 1284–1288 (2011)
28. L. Chen, C.Z. Yuan, H. Dou, B. Gao, S.Y. Chen, X.G. Zhang, Electrochim. Acta **54**, 2335–2341 (2009)
29. Z. Zhang, X. Zhao, J. Li, ChemNanoMat **2**, 196–200 (2016)
30. Y.Q. Zhao, D.D. Zhao, P.Y. Tang, Y.M. Wang, C.L. Xu, H.L. Li, Mater. Lett. **76**, 127–130 (2012)
31. G.P. Pandey, A.C. Rastogi, Electrochim. Acta **87**, 158–168 (2013)
32. V. Khomenko, E. Frackowiak, F. Béguin, Electrochim. Acta **50**, 2499–2506 (2005)
33. M.H. Yu, Y.X. Zeng, C. Zhang, X.H. Lu, C.H. Zeng, C.Z. Yao, Y.Y. Yang, Y.X. Tong, Nanoscale **5**, 10806–10810 (2013)
34. H.H. Zhou, H.J. Zhai, G.Y. Han, J. Mater. Sci. Mater. Electron. **27**, 2773–2782 (2016)
35. M. Jin, Y.Y. Liu, Y.L. Li, Y.Z. Chang, D.Y. Fu, H. Zhao, G.Y. Han, J. Appl. Polym. Sci. **122**, 3415–3422 (2011)
36. Q.Q. Zhou, Y.R. Li, L. Huang, C. Li, G.Q. Shi, J. Mater. Chem. A **2**, 17489–17494 (2014)
37. M. Szkoda, K. Trzciński, J. Rysz, M. Gazda, K. Siuzdak, A. Lisowska-Oleksiak, Solid State Ionics **302**, 197–201 (2017)
38. H.G. Wei, J.H. Zhu, S.J. Wu, S.Y. Wei, Z.H. Guo, Polymer **54**, 1820–1831 (2013)
39. C. Peng, J. Jin, G.Z. Chen, Electrochim. Acta **53**, 525–537 (2007)
40. H.Y. Mi, X.G. Zhang, X.G. Ye, S.D. Yang, J. Power Sources **176**, 403–409 (2008)
41. Y. Song, J.L. Xu, X.X. Liu, J. Power Sources **249**, 48–58 (2014)
42. J. Yan, E. Khoo, A. Sumboja, P.S. Lee, ACS Nano **4**, 4247–4255 (2010)
43. W.Y. Li, J.N. Xu, Y.S. Pan, L. An, K.B. Xu, G.J. Wang, Z.S. Yu, L. Yu, J.Q. Hu, Appl. Surf. Sci. **357**, 1747–1752 (2015)
44. W.F. Wei, X.W. Cui, W.X. Chen, D.G. Ivey, Chem. Soc. Rev. **40**, 1697–1721 (2011)
45. H.H. Zhou, G.Y. Han, Y.Z. Chang, D.Y. Fu, Y.M. Xiao, J. Power Sources **274**, 229–236 (2015)
46. H.H. Zhou, G.Y. Han, D.Y. Fu, Y.Z. Chang, Y.M. Xiao, H.J. Zhai, J. Power Sources **272**, 203–210 (2014)
47. H.H. Zhou, G.Y. Han, Electrochim. Acta **192**, 448–455 (2016)
48. H.G. Wei, Y.R. Wang, J. Guo, X.R. Yan, R. O'Connor, X. Zhang, N.Z. Shen, B.L. Weeks, X.H. Huang, S.Y. Wei, Z.H. Guo, ChemElectroChem **2**, 119–126 (2015)